Available online at www.sciencedirect.com

ScienceDirect

Procedia Engineering 207 (2017) 1976–1981

Procedia Engineering

www.elsevier.com/locate/procedia

International Conference on the Technology of Plasticity, ICTP 2017, 17-22 September 2017, Cambridge, United Kingdom

Experimental Verification of the Tension-Compression Asymmetry of the Flow Stresses of a High Strength Steel Sheet

Taiki Maeda[a], Nobuyasu Noma[b], Toshihiko Kuwabara[c,] *, Frédéric Barlat[d], Yannis P. Korkolis[e]

[a] *Department of Mechanical Systems Engineering, Faculty of Engineering, Tokyo University of Agriculture and Technology, 2-24-16 Nakacho, Koganei-shi, Tokyo 184-8588, Japan.*

[b] *Advanced Engineering Development Center, UNIPRES Co., 3-19-1, Shinyokohama, Kouhoku-ku, Yokohama 222-0033, Japan.*

[c] *Division of Advanced Mechanical Systems Engineering, Institute of Engineering, Tokyo University of Agriculture and Technology, 2-24-16 Nakacho, Koganei-shi, Tokyo 184-8588, Japan*

[d] *Graduate Institute of Ferrous Technology, Pohang University of Science and Technology, San 31 Hyoja-Dong, Nam-Gu, Pohang Gyeongbuk, 790-784, South Korea*

[e] *Department of Mechanical Engineering, University of New Hampshire, UNH Kingsbury Hall, Rm W131, 33 Academic Way, Durham, NH 03824, USA*

Abstract

The tension-compression asymmetry (TCA) of a dual phase steel sheet with a tensile strength of 980 MPa is measured using an in-plane uniaxial tension-compression testing apparatus. The TCA data within a logarithmic strain range of $0 \leq |\varepsilon| \leq 0.086$ are observed both in the rolling and transverse directions of the test material. Moreover, a novel testing apparatus for measuring a pure bending moment-curvature ($M-\kappa$) diagram is designed and manufactured. The measured $M-\kappa$ curves are consistent with those calculated taking into account the TCA of the stress-strain curve both in the rolling and transverse directions.

Peer-review under responsibility of the scientific committee of the International Conference on the Technology of Plasticity.

Keywords: High-Strength Steel; Tension-Compression Asymmetry; In-Plane Compression; Pure Bending

* Corresponding author. Tel.: +81-42-388-7083; fax: +81-42-385-7204
E-mail address: kuwabara@cc.tuat.ac.jp

1877-7058
Peer-review under responsibility of the scientific committee of the International Conference on the Technology of Plasticity.
10.1016/j.proeng.2017.10.1099

1. Introduction

The demand for advanced high-strength steel (AHSS) sheet is increasing in the automotive industry for the manufacture of environment-friendly and collision-safe cars. However, AHSSs are difficult materials to use in sheet metal forming processes, as they cause large springback to the press-formed parts after forming. In a bending process, thin material layers outside the neutral plane are in tension and those inside the neutral plane are in compression. The amount of springback is proportional to the bending moment [1], and the bending moment is determined from the in-plane tension-compression stress distribution in the thickness direction. Therefore, the predictive accuracy of the bending stress distribution in a bent sheet is of crucial importance for accurate springback prediction.

It is commonly assumed that the uniaxial tensile and compressive flow stresses of metals have the same magnitude (absolute value) when the absolute values of the tensile and compressive strains are identical to each other. However, this assumption is not always correct. For example, it is well known that the hcp metals exhibit tension/compression asymmetry (TCA). Another example is that a heavily cold rolled phosphor bronze sheet [2] and SUS304 austenitic stainless steel sheet [3] also exhibit the TCA caused by the Bauschinger effect and cross effect.

Other physical mechanisms of the TCA were investigated by several authors. Experimental studies have shown that the flow stress of some metals is clearly influenced by superimposed hydrostatic pressure, i.e. the flow stress increases with hydrostatic pressure. Such a pressure dependency of the flow stress has been observed mainly for iron-based metals [4, 5]. As a consequence, it is observed that the flow stress of iron-based metals is often clearly larger in uniaxial compression than in uniaxial tension. This phenomenon is known as the strength differential effect (SDE) [6]. Kuroda and Kuwabara [7] investigated the shear-band development in polycrystalline metal with the SDE and dilatancy, using a rate-dependent crystal-plasticity model with a fully three-dimensional, body-centered cubic, slip-system structure.

This study experimentally investigates the TCA of a 980 MPa dual phase steel sheet. In-plane uniaxial tension and compression responses of the test material were measured using a comb-type testing device developed by one of the current authors [8]. The stress-strain (ss) curves of the test material under monotonic tension and compression were precisely measured to obtain accurate knowledge of the SDE. These measured ss curves were approximated using analytical functions to calculate the bending moment and to validate the bending moment to be experimentally measured later. As a second part of the experimental study, pure bending tests were performed and bending moment M – curvature κ diagrams were measured precisely for the test material. Moreover, the measured $M - \kappa$ diagrams were compared with those calculated using the stress-strain curves obtained from the in-plane tension-compression tests to verify the characterized material responses under the monotonic loading.

2. Experimental methods

2.1. Material

The test material used in this study was a 1.2 mm thick dual phase steel sheet with a tensile strength of 980 MPa (DP980).

2.2. In-plane tension-compression experiment

In order to measure the tension-compression asymmetry of the test material, in-plane uniaxial tension and compression tests were performed. Fig. 1(a) shows the comb-type dies developed for application of continuous in-plane stress reversal to a sheet specimen. The dies are similar in geometry to those developed in [8], but the rigidity was increased. Lower and upper comb-type dies are installed in the testing apparatus, see [8]. Lower die 1 is fixed to the lower plate of a die-set and lower die 2 is fixed to a table on a slide rail that enables the die to move smoothly in the horizontal direction. A sheet specimen is set on lower dies 1 and 2 and both ends of the specimen are clamped by chucking plates. Upper dies 1 and 2 are placed on the specimen so that the four positioning pins fixed to the lower dies align with the holes of the upper dies. Accordingly, the movement of the upper dies is synchronized with

that of the lower dies. Lower die 2 is actuated in the horizontal direction by a servo-controlled hydraulic cylinder, so that continuous in-plane stress reversals are applied to the specimen. A vertical hydraulic cylinder exerts a constant blank-holding force on the specimen through the upper dies and the cylindrical rollers lying between the upper dies and the blank-holding platen. The specimen can thus be compressed in the longitudinal direction without buckling.

Fig. 1(b) shows the dimensions of the specimen used in the in-plane tension-compression experiments. According to a FEA of the specimen, with the strain measurement position shown in Fig. 1(b), the stress measurement error was estimated to be less than 1 % [9]. In order to prevent buckling of the specimen during in-plane compression, a blank-holding pressure of 7.1 MPa was applied to the specimen. The specimen was lubricated on both sides with Vaseline and Teflon sheets (0.1 mm thickness) to prevent the specimen from galling the dies, resulting in reduction of the coefficient of friction to 0.02.

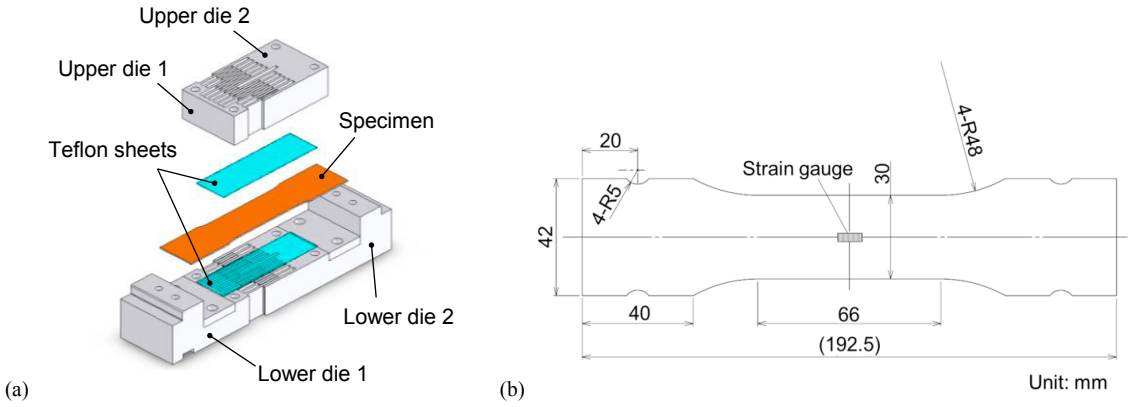

Fig. 1 (a) Configuration of the dies for in-plane compression test. (b) Geometry of specimen for in-plane compression test.

It should be noted that the frictional forces between the dies and specimen have little effect on the measured stress values, as is shown in [2]. This is the significant advantage of this testing device over other reported in-plane compression testing devices [10-12], in which the predetermined frictional force must be subtracted from the measured force data; such a procedure may cause unavoidable uncertainty in the accuracy of the measured stress data.

2.3. Pure bending experiment

Fig. 2 shows a schematic diagram of the pure bending testing apparatus designed and built in this study. Both ends of the specimen were fixed to two fan-shaped blocks. A thin steel wire is wound around the circular side of each block. The blocks can rotate around the rotating axis when tension is applied to the wire. Thus, the specimen is bent under a pure bending moment M and is free from axial force during the bending process, as the rotating axes of the blocks are fixed to sliding rails that can move freely in the horizontal direction during the bending process. The curvature κ of the specimens during bending tests was measured using strain gauges (Kyowa Electronic

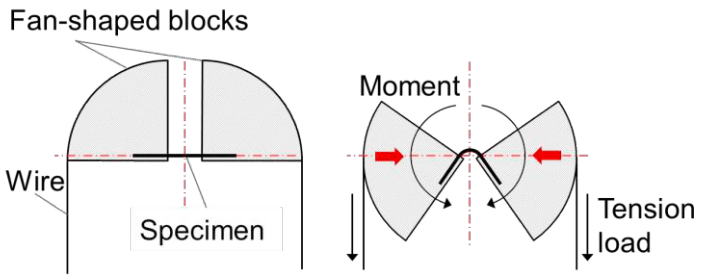

Fig. 2 (b) Schematic illustration of pure bending test.

Instruments Co., KFG-1N-120-C1-11) glued onto both sides of the specimen with a length and width of the gauge section was 10 x 1.5 mm^2. The bending specimens were fabricated using wire-cut electrical discharge machining. A finite element analysis was performed to confirm that the magnitude of the stress in the width direction of the specimen during the bending test was approximately 1 % of the maximum bending stress. Thus, the gauge section of the bending specimen during the bending test can be assumed to be in a uniaxial stress state.

3. Experimental results

Fig. 3(a) compares the stress-strain curves measured in the tension-compression tests in the TD of the test material. The tensile flow stress σ^{T} and compressive flow stress σ^{C} do not coincide with each other, clearly showing the TCA. σ^{C} is consistently larger than σ^{T}, and $\left(\left|\sigma^{\mathrm{C}}\right|-\sigma^{\mathrm{T}}\right)/\sigma^{\mathrm{T}}\times 100$ is 6.2 % at $|\varepsilon|=0.086$. Similar results were obtained also for the RD. In the RD $\sigma^{\mathrm{T}}>\left|\sigma^{\mathrm{C}}\right|$ for $|\varepsilon|\leq 0.009$. This was caused by the Bauschinger effect, as a small tensile plastic strain had been applied to the material during the cold rolling process. On the other hand, $\sigma^{\mathrm{T}}<\left|\sigma^{\mathrm{C}}\right|$ for $|\varepsilon|>0.009$, and the $\left(\left|\sigma^{\mathrm{C}}\right|-\sigma^{\mathrm{T}}\right)/\sigma^{\mathrm{T}}\times 100$ is 5.2 % at $|\varepsilon|=0.086$.

Fig. 3(a) also shows the calculated curves approximating the measured ones using analytical functions; see Appendix A1 for the details of the functions. They were used to calculated the $M-\kappa$ curves; see Appendix A2 for the details of the calculation procedures.

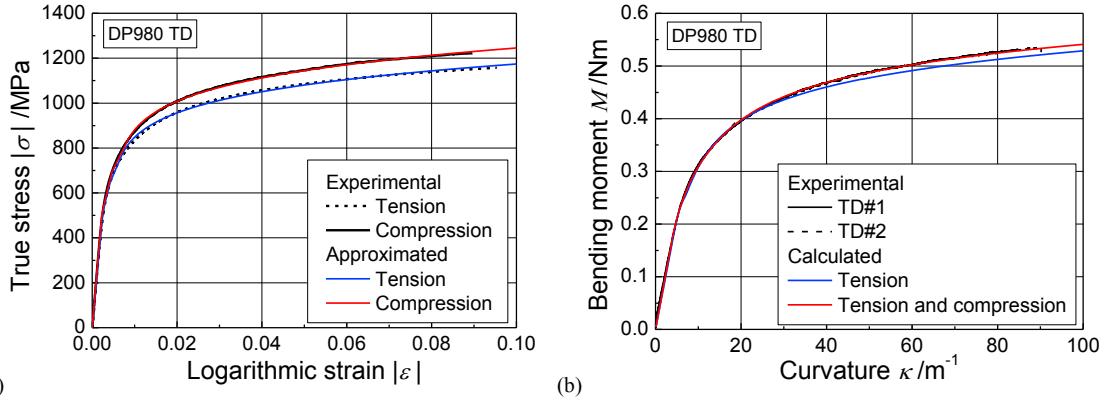

Fig. 3 (a) Comparison of the true stress vs. logarithmic strain curves between tension and compression in the TD. (b) Comparison of measured and calculated bending moment-curvature curves for (a) RD and (b) TD.

Fig. 3(b) compares the experimental and calculated $M-\kappa$ curves in the TD. The two experimental curves are consistent with each other; thus, a reproducibility of the experimental data was confirmed. The blue curve shows the bending moment calculated using only the tensile ss curve shown in Fig. 3(a), while the red curve shows that moment calculated by taking into account the TCA; M was calculated using the tensile and compressive ss curves, shown in Fig. 3(a), for the thin layers subjected to tensile and compressive strains, respectively. The latter (red curve) is clearly higher than the former (blue curve) for a range of $\kappa\geq 30$ m^{-1}. This is because the compressive flow stresses are larger than the tensile flow stresses, as shown in Fig. 3(a). The measured $M-\kappa$ curves are consistent with the red curves. Thus, the ss curves showing the TCA shown in Fig. 3(a) are verified. Following the same procedures as described above, the ss curves showing the TCA in the RD have been also verified.

4. Conclusions

(1) For the tension-compression tests in the TD $|\sigma^{\mathrm{C}}|$ are consistently larger than σ^{T} for $0<|\varepsilon|\leq 0.086$. At $|\varepsilon|=0.086$, $|\sigma^{\mathrm{C}}|$ is larger than σ^{T} by 6.2 %.

(2) In the RD $\sigma^{\mathrm{T}} > \left|\sigma^{\mathrm{C}}\right|$ for $|\varepsilon| \leq 0.009$ while $\sigma^{\mathrm{T}} < \left|\sigma^{\mathrm{C}}\right|$ for $|\varepsilon| > 0.009$, and the $\left(\left|\sigma^{\mathrm{C}}\right| - \sigma^{\mathrm{T}}\right)/\sigma^{\mathrm{T}} \times 100$ is 5.2 % at $|\varepsilon| = 0.086$.

(3) The experimental $M-\kappa$ diagrams were consistent with those calculated by taking into account the TCA experimentally observed. Thus, the TCA of the test material was successfully verified.

Appendix

A.1. Approximation of the tension-compression stress-strain curves using analytical functions

The uniaxial tension-compression stress-strain curves shown in Fig. 3(a) were approximated using analytical functions as follows:

$$\begin{cases} \varepsilon \leq \varepsilon_{\mathrm{hooke}} : \sigma = 1000E\varepsilon \,/\, \mathrm{MPa} \\ \varepsilon_{\mathrm{hooke}} < \varepsilon \leq \varepsilon_{\mathrm{mid}} : \sigma = \dfrac{1000E\varepsilon_{\mathrm{hooke}} - \sigma_{\mathrm{mid}}}{\varepsilon_{\mathrm{hooke}} - \varepsilon_{\mathrm{mid}}}(\varepsilon - \varepsilon_{\mathrm{hooke}}) + 1000E\varepsilon_{\mathrm{hooke}} \,/\, \mathrm{MPa} \\ \varepsilon_{\mathrm{mid}} < \varepsilon < \varepsilon_{\mathrm{swift}} : \sigma = \dfrac{\sigma_{\mathrm{mid}} - c(\alpha + \varepsilon_{\mathrm{swift}})^n}{\varepsilon_{\mathrm{mid}} - \varepsilon_{\mathrm{swift}}}(\varepsilon - \varepsilon_{\mathrm{mid}}) + \sigma_{\mathrm{mid}} \,/\, \mathrm{MPa} \\ \varepsilon_{\mathrm{swift}} \leq \varepsilon : \sigma = c\left(\varepsilon_0 + \varepsilon\right)^n \,/\, \mathrm{MPa} \end{cases} \tag{A1}$$

Table A1 shows the values of the parameters in Eq. (A1).

Table A1 Parameters of DP980 steel for stress calculation

Direction	Loading mode	*Young's modulus* *E* /GPa	*r*-value*	*c* ** /MPa	*n* **	ε_0 **	$\varepsilon_{\mathrm{hooke}}$	$\varepsilon_{\mathrm{swift}}$	$\varepsilon_{\mathrm{mid}}$	σ_{mid} /MPa
RD	Tension	186	0.69	1518	0.12	-0.0049	0.0026	0.0072	0.0045	627
	Compression	189	0.65	1612	0.12	-0.0068	0.0024	0.0092	0.0058	665
TD	Tension	207	0.96	1527	0.11	-0.0048	0.0025	0.0070	0.0042	648
	Compression	226	0.91	1646	0.12	-0.0057	0.0022	0.0085	0.0046	694

*Measured at uniaxial nominal strain $\varepsilon_{\mathrm{N}} = 0.09$ for tension and at logarithmic strain $|\varepsilon| = 0.09$ for compression

**Approximated using $\sigma = c(\varepsilon_0 + \varepsilon)^n$ at $\varepsilon = \varepsilon_{\mathrm{swift}} \sim 0.06$

A.2. Method of Calculating Bending Moment-Curvature Diagram

The sheet thickness was divided into 100 thin layers of equal thickness. The *i*-th layer counted from the concave surface of the bent specimen is denoted as "layer-*i*" and the subscript *i* is attached to values related to the layer-*i*.

The following terms were assumed in calculating the bending moment-curvature diagram:

(i) The stretching force in the *x*-direction is assumed to be zero during the bending process.

(ii) All layers in the sheet are subjected to uniaxial tension; σ is the only non-zero stress component in the sheet.

(iii) The cross-section of the sheet remains planar and normal to the *x*-axis during the bending process.

(iv) All layers in the sheet follow stress-strain responses as determined by Eq. (A1) during the bending process.

The bending strain ε and bending stress σ of layer-*i* were determined as follows. The radius of the layer at which $\varepsilon = 0$ is denoted as r_n, and its *y*-coordinate is assumed to be zero, $y_n = 0$, and the bending strain ε_i of layer-*i* can be determined from:

$$\varepsilon_i = \ln(1 + y_i / r_n) . \tag{A2}$$

Substituting Eq. (A2) into Eq. (A1), the corresponding stress value σ_i for layer-*i* can be determined.

Since the stretching force applied to the sheet is zero, the equilibrium equation in the x-direction must be satisfied as:

$$\sum_{i=1}^{100} \sigma_i w_i \Delta y_i = 0 , \tag{A3}$$

where w_i and Δy_i are the width and thickness of layer-*i*, respectively.

The value of r_n in Eq. (A2) was iteratively determined so that Eq. (A3) was satisfied. The bending moment M, corresponding to r_n was determined as:

$$M = \sum_{i=1}^{100} \sigma_i w_i y_i \Delta y_i . \tag{A4}$$

The curvature κ was calculated as $\kappa = 1/r_n$. In the pure bending experiment it was determined as:

$$\kappa = \frac{\left|\varepsilon_{\mathrm{N}}^{\mathrm{C}}\right| + \varepsilon_{\mathrm{N}}^{\mathrm{T}}}{t} , \tag{A5}$$

where $\varepsilon_{\mathrm{N}}^{\mathrm{T}}$ and $\varepsilon_{\mathrm{N}}^{\mathrm{C}}$ are the magnitudes of the bending strains at the convex and concave sides of the bent specimen, respectively, measured using strain gauges.

References

[1] Z. Marciniak, J.L. Duncan, S.J. Hu, Mechanics of Sheet Metal Forming, second ed., Butterworth-Heinmann, MA, 2002.

[2] T. Kuwabara, Y. Kumano, J. Ziegelheim, I. Kurosaki, Tension-compression asymmetry of phosphor bronze for electronic parts and its effect on bending behavior, Int. J. Plasticity 25 (2009) 1759–1776.

[3] T. Kuwabara, R. Saito, T. Hirano, N. Oohashi, Tension-compression asymmetry of SUS304 stainless sheet for electronic parts and its effects on bending and springback behavior, Tetsu-to-Hagané 95 (2009) 732–739.

[4] W.A. Spitzig, R.J. Sober, O. Richmond, Pressure dependence of yielding and associated volume expansion in tempered martensite, Acta Metall. 23 (1975) 885–893.

[5] W.A. Spitzig, R.J. Sober, O. Richmond, The effect of hydrostatic pressure on the deformation behavior of maraging and HY-80 steels and its implications for plasticity, Metall. Trans. A7 (1976) 1703–1710.

[6] W.C. Leslie, R.J. Sober, The strength of ferrite and of martensite as functions of composition, temperature and strain rate, Trans. ASM 60 (1967) 459–484.

[7] M. Kuroda, T. Kuwabara, Shear-band development in polycrystalline metal with strength-differential effect and plastic volume expansion, Proc. Roy. Soc. Lond. A 458 (2002) 2243–2259.

[8] T. Kuwabara, K. Nagata, T. Nakako, Measurement and analysis of the Bauschinger effect of sheet metals subjected to in-plane stress reversals, in: Torralba, J. M. (Ed.), Proc. AMPT '01, Univ. Carlos III de Madrid, Madrid, 2001, pp. 407-412.

[9] N. Noma, T. Kuwabara, Specimen geometry optimization for in-plane reverse loading test of sheet metal and experimental validation, Steel Research International, Special Edition: 14th Metal Forming, 2012, pp. 1283-1286.

[10] N. Iwata, M. Matsui, T. Kato, K. Kaneko, H. Tsutamori, N. Suzuki, M. Gotoh, Numerical prediction of spring-back behavior of a stamped metal sheet by considering material nonlinearity during unloading, in: Mori, K. (Ed.), Proc. 7th Int. Conf. Numerical Methods in Industrial Forming Processes. Balkema, Lisse, 2001, pp. 693–698.

[11] R.K. Boger, R.H.Wagoner, F. Barlat, M.G. Lee, K. Chung, Continuous, large strain, tension/compression testing of sheet material, Int. J. Plasticity 21 (2005) 2319–2343.

[12] J. Cao, W. Lee, H.S. Cheng, M. Seniw, H.-P. Wang, K. Chung, Experimental and numerical investigation of combined isotropic-kinematic hardening behavior of sheet metals, Int. J. Plasticity 25 (2009) 942–972.